

Short Note

Segmentally Iterative Ray Tracing in Complex 2D and 3D Heterogeneous Block Models

by Tao Xu, Zhongjie Zhang, Ergen Gao, Guoming Xu, and Lian Sun

Abstract We describe a complex geologic model as an aggregate of arbitrarily shaped blocks separated by cubic splines in 2D and triangulated interfaces in 3D. Recently we have introduced a segmentally iterative ray-tracing (SIRT) method based on Fermat's principle of stationary travel time, which has been documented to be robust and fast for a complex block model with a constant velocity defined in each block. In this work, we extend the constant velocity to a generally continuous distribution with an analytical expression of travel time, and develop SIRT in the redefined velocity distribution. As a three-point perturbation scheme, SIRT requires an explicit analytical travel time between two intersection points expressed as a function of coordinates of the two points. In these situations, we derive a general midpoint perturbation formula, and further a detailed perturbation formula for familiar media with a constant velocity gradient. SIRT is a scheme in which we perturb the intersection points of an initial-guess ray path in sequence by the first-order explicit formulas instead of using traditional iterative methods. A key consideration is the fact that the number of intersection points may be variable during the iteration process. Numerical tests demonstrate that SIRT is effective in implementing kinematic two-point ray tracing in complex 2D and 3D heterogeneous media.

Introduction

Two-point ray tracing is crucial to earthquake location, seismic tomography, migration, seismic acquisition, and many other applications. Previously reported methods include shooting (Langan *et al.*, 1985; Virieux and Farra, 1991; Sun, 1993; Sambridge *et al.*, 1995) and bending (Julian and Gubbins, 1977; Aki and Richards, 1980; Thurber and Ellsworth, 1980; Pereyra *et al.*, 1980; Keller and Perozzi, 1983; Um and Thurber, 1987; Prothero *et al.*, 1988; Pereyra, 1992; Mao and Stuart, 1997; Xu *et al.*, 2001, 2006). Other methods include wavefront techniques (Vinje *et al.*, 1993, 1996, 1999), graph theory (Moser, 1991; Zhang *et al.*, 2000; Zhao *et al.*, 2004), and simulated annealing (Velis and Ulrych, 1996, 2001). A good summary of these methods can be found in Červený (1988, 2001).

Most of the previously mentioned tracing methods are based on models parameterized in grids or cells (Langan *et al.*, 1985; Vidale, 1988, 1990; Moser, 1991), layers (Keller and Perozzi, 1983; Zelt and Smith, 1992; GuiZiou *et al.*, 1996; Mao and Stuart, 1997; Rawlinson *et al.*, 2001; Zhang *et al.*, 2003, 2005; Zhang and Klemperer, 2005; Zhang and Wang, 2007), and arbitrarily shaped blocks (Gjøystdal *et al.*, 1985; Pereyra, 1992; Xu *et al.*, 2001, 2006, 2008). A fine grid-based model can be a good approximation to reality;

however, memory space and tracing time increase dramatically with node spacing reduced for accuracy purposes. In some situations, a horizontally stratified model is fairly efficient in describing geologic structures and very convenient for ray tracing because the process of rays passing through and returning through the overburden layers in sequence is easy to implement. Layered parameterization is very difficult in the case of more general complex structure (Fig. 4a), and hence inapplicable for some cases in realistic seismic exploration. A block model can faithfully represent such complex structures as faults, pinch-out layers, intrusive tectonics, and lens, whereas model parameterization and corresponding ray tracing are more complex.

Recently, we developed a block model and introduced a robust segmentally iterative ray-tracing (SIRT) method for fast ray tracing in complex media (Xu *et al.*, 2006). We perturb the intersection points of an initial-guess ray path in sequence by a first-order explicit formula. A flaw in this scheme is that the velocity in each block must be defined as a constant. Heterogeneous blocks can be approximated by several small blocks, however, this is not efficient for even constant gradient velocity blocks, thus routine use is limited for realistic applications. This article is an extension of our

previous work. We redefine the velocities to be generally continuous in the blocks with an analytical expression of travel time and develop SIRT to suit these models with redefined velocities. Usually, SIRT can also be applied in the same way for any velocity distribution, for which we have explicit analytical formulas for the travel time and the ray between two points within the block. Then, a general perturbation formula can also be derived. Considering that the great majority of current applications employ the constant gradient velocity distribution (with an arbitrarily oriented gradient), we especially derive a detailed perturbation formula for the constant gradient velocity distributions, which is similar to but more general than that for constant velocity distributions.

Model Parameterization

2D and 3D Block Models

We describe 2D and 3D block model structures in the same way as [Xu et al. \(2001, 2006, 2008\)](#). A 2D structure is represented hierarchically as area \rightarrow element \rightarrow edge \rightarrow point. Geologic elements are closed regions separated by edges, which are cubic splines interpolated by discrete points. In 3D, the block hierarchical structure is represented as volume \rightarrow block \rightarrow interface \rightarrow triangle \rightarrow point. Geologic media are described as an aggregate of arbitrarily shaped geologic blocks, which are separated by triangulated interfaces.

The triangulated interface has several advantages compared to B -spline surface patches, which was widely used. First, discrete points need not be defined in a rectangular domain. Second, no gaps would be produced in linking triangulated patches, whereas strict constraints are requisite in B -spline linking. Third, modifying and eliminating in accurate geological nodes is easily implemented. Furthermore, the intersection between a line and a triangle can be computed analytically, as opposed to iterative techniques for ray/ B -spline patch intersection ([Virieux and Farra, 1991](#); [Rawlinson et al., 2001](#)). Hence, large numbers of ray/interface intersections can be computed quickly to save tracing time.

The disadvantage of the triangulated interface is that it is less smooth. Normal vectors hold constants inside a triangle and vary abruptly across the linked boundary of two triangles that are not in the same plane. As a result, a reflected or transmitted ray may change direction abruptly across linked boundaries. It is especially awful for such ray-tracing methods that rely on nearby ray trajectories to vary smoothly to find an optimal solution. To avoid this difficulty, we have introduced an algorithm to redefine normal vectors at arbitrary points on an interface so that normal vectors are continuous on the whole interface. Triangulated interfaces are also applied in the well-known GOCAD system ([Mallet 1989, 1992](#)). For more detailed advantages and disadvantages of block models with triangulated interfaces, see [Xu et al. \(2006\)](#).

Velocity Distribution in the Blocks

In isotropic media, velocities may be defined to be homogeneous, constant gradient ([Slotnick, 1936](#); [Rawlinson et al., 2001](#)), exponential ([Slotnick, 1936](#)), conic ([Ravve and Koren, 2007](#)), and typically analytical ([Al-Chalabi, 1997](#)). Homogeneous models are simple but still applied frequently. Conic models are typically described for some subsurface-sediment basins. Usually, more complex realistic models assume that the velocity increases linearly with depth. This is commonly accepted and often confirmed by measurements of thin clastic rocks. After long tectonic evolution, horizontal beds may become dipping ones or much more complex geologic blocks ([Fig. 4a](#)). Furthermore, the velocity may deviate from the constant gradient increase with vertical depth; for example, there is a tilted gradient rather than a vertical gradient in a tilted sediment basin. In this case, the velocity distribution may vary generally with constant gradient as

$$v(\mathbf{x}) = v_0 + \mathbf{k} \cdot \mathbf{x}, \quad (1)$$

where \mathbf{k} is the gradient vector and \mathbf{x} is the position point.

In this article, we extend the velocity defined in individual blocks to a generally continuous distribution $v(\mathbf{x})$ with an analytical expression of travel time, and further to a generally continuous distribution with a constant gradient described as equation (1). When $\mathbf{k} = -k\mathbf{z}$ (up is positive), the velocity changes with a constant gradient with depth and is constant when $\mathbf{k} = 0$.

Ray Trajectories and Travel Times

Seismic ray travel time in an arbitrary velocity distribution can be expressed as integral form

$$t = \int \frac{ds}{v(\mathbf{x})}. \quad (2)$$

Such form may not be an explicit analytical expression with the exception of time-depth relationships for several analytical functions ([Al-Chalabi, 1997](#)). For a generally constant gradient velocity model (with an arbitrarily oriented gradient), the travel time between two points \mathbf{x} and \mathbf{y} is given as ([Červený, 2001](#), chapter 3.7.2)

$$t(\mathbf{x}, \mathbf{y}) = \frac{1}{k} \text{arc cosh } p, \quad (3)$$

with

$$p = 1 + \frac{k^2 r^2}{2v(\mathbf{x})v(\mathbf{y})}, \quad r = \|\mathbf{x} - \mathbf{y}\|, \quad k = \|\mathbf{k}\|. \quad (4)$$

In such a velocity distribution, the ray trajectory is a circular arc and hence can be obtained in terms of the geometry property (details in [Appendix A](#)). Some explicit expressions of ray trajectory and travel time are presented with the intermediate variables, direction vectors tangent to the ray trajectory, in a constant gradient velocity distribution with depth ([Telford et al., 1990](#); [Rawlinson et al., 2001](#)). Such expressions are beneficial for the initial value problem, but are not

suitable for a general velocity distribution with constant gradient.

Ray-Tracing Method

Segmentally Iterative Ray-Tracing (SIRT) Method

Bending methods are usually advantageous over shooting methods when the receiver positions are ill-behaved functions of the shooting angles. Much work has been reported (Červený, 2001). Numerical methods are adopted by Julian and Gubbins (1977). A structural perturbation scheme using continuation or homotopy methods is presented by Keller and Perozzi (1983). Recently, we introduced a segmentally iterative ray-tracing method to suit complex block models both in 2D (Xu *et al.*, 2001) and in 3D (Xu *et al.*, 2006). Application of the stationary travel-time principle to three successive points along a ray path results in a perturbation formula for improving the midpoint in sequence during SIRT. The perturbation formula is a first-order explicit one instead of a traditional iterative method (the bisection method, Zhao *et al.*, 1992), which can speed up ray tracing convergence. As a local updating scheme, SIRT usually requires less computation per iteration than those solving a linear system of equations. Another three-point perturbation scheme, namely the pseudobending method (Um and Thurber, 1987), also employs an explicit perturbation formula. This scheme can only be applied to continuous velocity distributions. It fails to work when velocity discontinuities exist.

SIRT requires an explicit analytical travel time between two intersection points expressed as a function of coordinates of the two points. In such continuous velocity distributions, a general midpoint perturbation formula can also be derived as follows.

General Perturbation Formula for Generally Continuous Velocity Distributions

As shown in Figure 1, P_0 , P_1 , and P_2 are successive intersection points along a ray trajectory. The midpoint P_1 is situated on the surface described by two parameters as

$$\mathbf{x} = \mathbf{x}(s, t). \quad (5)$$

Because P_0 and P_2 are fixed, the travel time is the function of the midpoint coordinates $\mathbf{x}(\xi, \eta)$ if the travel time between two points is an explicit function of the coordinates of the two points, which is described as

$$T = t_1(P_0, \mathbf{x}) + t_2(\mathbf{x}, P_2). \quad (6)$$

To satisfy the stationary travel-time principle, the partial derivative formulas at the improved midpoint $(\xi + \Delta s, \eta + \Delta t)$ are

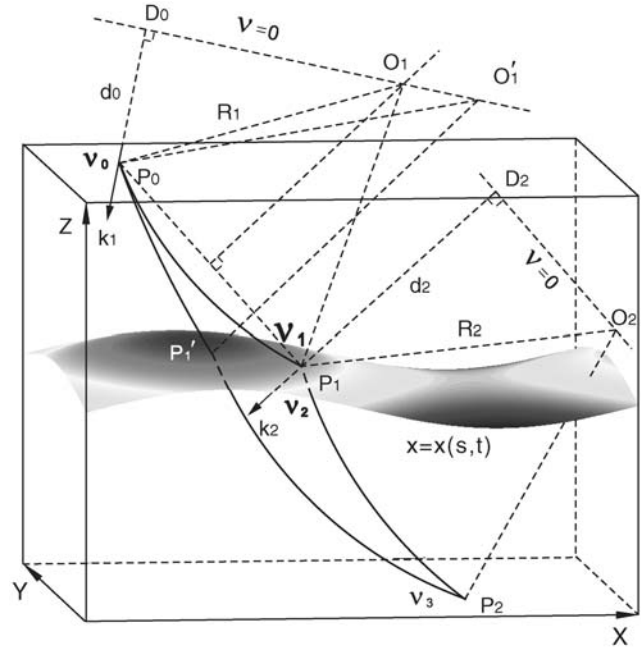


Figure 1. The sketch illustrating ray trajectory P_0P_1 obtained by the geometry property and for modifying the middle point P_1 of two successive segments of a trajectory in a constant gradient velocity model. The center O_1 of the first arc is obtained by the cross of velocity-zero-plane marked with $v = 0$ and the perpendicular bisector of the line segment P_0P_1 . Note that gradient vector \mathbf{k}_1 and vectors \mathbf{O}_1P_0 , \mathbf{O}_1P_1 lie in the same plane. Midpoint P_1 is updated by an improved point P_1' with a perturbation formula.

$$\left. \frac{\partial T}{\partial s} \right|_{(s=\xi+\Delta s, t=\eta+\Delta t)} = 0, \quad \left. \frac{\partial T}{\partial t} \right|_{(s=\xi+\Delta s, t=\eta+\Delta t)} = 0. \quad (7)$$

Using only the first term of a Taylor series, we obtain

$$\begin{aligned} \frac{\partial T}{\partial x_i} x_{is} + \left(\frac{\partial^2 T}{\partial x_i \partial x_j} x_{is} x_{js} + \frac{\partial T}{\partial x_i} x_{iss} \right) \Delta s \\ + \left(\frac{\partial^2 T}{\partial x_i \partial x_j} x_{is} x_{jt} + \frac{\partial T}{\partial x_i} x_{ist} \right) \Delta t = 0, \\ \frac{\partial T}{\partial x_i} x_{it} + \left(\frac{\partial^2 T}{\partial x_i \partial x_j} x_{it} x_{js} + \frac{\partial T}{\partial x_i} x_{its} \right) \Delta s \\ + \left(\frac{\partial^2 T}{\partial x_i \partial x_j} x_{it} x_{jt} + \frac{\partial T}{\partial x_i} x_{itt} \right) \Delta t = 0, \end{aligned} \quad (8)$$

where the superscript i denotes three coordinates of the midpoint. We easily obtain the first-order perturbation formula, which is the same whether the midpoint is a reflection or transmission point as follows

$$\begin{aligned} \Delta s &= \frac{U_{13}U_{22} - U_{23}U_{12}}{U_{11}U_{22} - U_{12}U_{21}}, \\ \Delta t &= \frac{U_{11}U_{23} - U_{21}U_{13}}{U_{11}U_{22} - U_{12}U_{21}}, \end{aligned} \quad (9)$$

where

$$\begin{aligned}
U_{11} &= \frac{\partial^2 T}{\partial x_i \partial x_j} x_{is} x_{js} + \frac{\partial T}{\partial x_i} x_{iss}, \\
U_{12} &= \frac{\partial^2 T}{\partial x_i \partial x_j} x_{is} x_{jt} + \frac{\partial T}{\partial x_i} x_{ist}, & U_{13} &= -\frac{\partial T}{\partial x_i} x_{is}, \\
U_{21} &= \frac{\partial^2 T}{\partial x_i \partial x_j} x_{it} x_{js} + \frac{\partial T}{\partial x_i} x_{its}, \\
U_{22} &= \frac{\partial^2 T}{\partial x_i \partial x_j} x_{it} x_{jt} + \frac{\partial T}{\partial x_i} x_{itt}, & U_{23} &= -\frac{\partial T}{\partial x_i} x_{it}, \\
x_{is} &= \frac{\partial x_i}{\partial s}, & x_{it} &= \frac{\partial x_i}{\partial t}, & x_{iss} &= \frac{\partial^2 x_i}{\partial s^2}, \\
x_{ist} &= x_{its} = \frac{\partial x_i}{\partial s} \frac{\partial x_i}{\partial t}, & x_{itt} &= \frac{\partial^2 x_i}{\partial t^2}.
\end{aligned} \tag{10}$$

Substitute the position $(\xi + \Delta s, \eta + \Delta t)$ for the primary position (ξ, η) directly if the improved midpoint falls on the original interface. Otherwise, additional judgment is needed to determine whether intersection points should be added or removed, as discussed in the next section.

For a surface patch in general form, such as $f(x, y, z) = 0$, there are small differences in the perturbation formulae. We can define $s = x, t = y$, then

$$\begin{aligned}
x_{1s} &= 1, & x_{2s} &= 0, & x_{3s} &= \frac{\partial z}{\partial x}, \\
x_{1t} &= 0, & x_{2t} &= 1, & x_{3t} &= \frac{\partial z}{\partial y}, \\
x_{iss} &= x_{ist} = x_{its} = x_{itt} = 0, & (i &= 1, 2), \\
x_{3ss} &= \frac{\partial^2 z}{\partial x^2}, & x_{3st} &= x_{3ts} = \frac{\partial^2 z}{\partial x \partial y}, & x_{3tt} &= \frac{\partial^2 z}{\partial y^2}.
\end{aligned} \tag{11}$$

For any given position on the interface, we can redefine the normal vectors by an algorithm (Xu *et al.*, 2006). Suppose the unit normal vector to be $\mathbf{n}(n_1, n_2, n_3)$, then we can easily obtain that vector $\mathbf{n}(n_1, n_2, n_3)$ and vector $\mathbf{n}_2(-\frac{\partial z}{\partial x}, -\frac{\partial z}{\partial y}, 1)$ have the uniform directions. Thus,

$$\frac{\partial z}{\partial x} = -\frac{n_1}{n_3}, \quad \frac{\partial z}{\partial y} = -\frac{n_2}{n_3}. \tag{12}$$

Note that we should consider the condition that n_3 is very close to zero. Because the normal vectors change linearly with the change of the coordinates of the position inside a triangle, the second-order partial derivatives hold the constants inside the triangle.

Substituting elements in equation (10) into equations (11) and (12) will result in the perturbation formulae in general form.

Equation (9) is a general form of the perturbation formula. As shown in equations (6) and (7), SIRT requires an explicit analytical travel time between two intersection points; for example, the travel time between two points of

a straight line in homogeneous media is the simplest case. The time-depth relationships for several analytical velocity functions are just 1D in depth (Al-Chalabi, 1997). Taking account of the fact that the familiar velocity distribution with constant gradient allows an analytical travel time, is the key consideration in this article. The exact perturbation formula is displayed in Appendix B.

Adaptability of SIRT in the Block Models with Constant Gradient Velocity Distributions

That shooting is relatively slow has been studied and documented in Xu *et al.* (2006), which is the same for the velocity distributions with constant gradient. Though numerical methods (Červený, 2001) and the pseudobending technique (Um and Thurber, 1987) are robust for generally continuous velocity distributions, a large number of steps or iterations are needed to approach a simple analytical arc for a velocity distribution with constant gradient. More steps and iterations are necessary for a higher precision. Thus, it is very time-consuming to obtain an approximate circular ray. This may not be realistic for some field work, such as seismic acquisition, which has a high requirement of the tracing speed. However, SIRT is especially efficient for constant gradient velocity models that are widely used, because a segmental ray trajectory is analytical inside a block and the intersection points situated on the interfaces are updated directly by a first-order explicit formula instead of an iterative technique (Zhao *et al.*, 1992). Because ray-tracing schemes involve modifying many intersection points, our tracing scheme can save considerable time.

In layered media, bending methods can involve updating the positions of intersection points simultaneously (Blais, 1985; Mao and Stuart, 1997). But in complex block models, the number of intersection points in a ray can be increased or decreased during the process of iterations, a phenomenon that does not occur in layered models. Additional judgments and operations should be automatically considered in the program, which are important and complex in SIRT in complex 2D and 3D block models. The main principle has been presented (Xu *et al.*, 2006). For a typical case such as a pinch-out layer, when the length of a segmental ray linked to the modified intersection point is less than a specified precision and the improved distance is also less than another specified precision, the operation of removing correlative intersection points should be performed automatically. This can prevent the well-known ray aggregation effect of reflective point, generated by other methods such as shooting, from occurring in pinch-out layers, thus improving seismic acquisition and migration. For simplification in ray tracing, we update the midpoints segmentally instead of simultaneously and add or remove intersection points as necessary. The use of the local perturbation scheme allows the method to be compatible with a wide variety of structures.

The procedure of SIRT in the constant gradient velocity blocks is similar to that in the constant velocity blocks.

However, it is more general, complex, and time-consuming due to the following issues: First, the perturbation formulae are lengthier and include log mathematic operators. Second, computing an analytical circular ray and circular ray/interface intersections as opposed to computing a straight line and line/interface intersections requires significantly more computation, especially for the shooting methods that rely on much more calculations of ray/interface intersections. Third, in complex block models, the ray-tracing scheme usually requires more automatic judgments about whether a segmental circular ray intersects other interfaces (plane triangles) in the block the segmental ray passes through. This is, because a circular ray tends to easily intersect other interfaces in the block; the intersection point can also be obtained with the judgment of the area coordinate (Xu *et al.*, 2006).

Synthetic Data Examples

The SIRT Schemes in the Heterogeneous Models

As a bending method, SIRT requires the initial-guess ray paths, generally obtained by shooting, for a source-receiver pair in both homogenous and heterogeneous velocity models. A group of rays are try-shot at a proper angle range in both vertical and horizontal planes and form a set of emergence triangles according to a certain rule on the surface (Fig. 2a) (Xu *et al.*, 2004, 2006, 2008). As Figure 2a shows, with the aid of area coordinates (Xu *et al.*, 2004, 2006), it can easily and rapidly determine the triangle where a target receiver P is situated. When the receiver P is located at the emergence triangle BEF , the shooting ray tracing is a process to update shooting angles so that the rays are directed toward

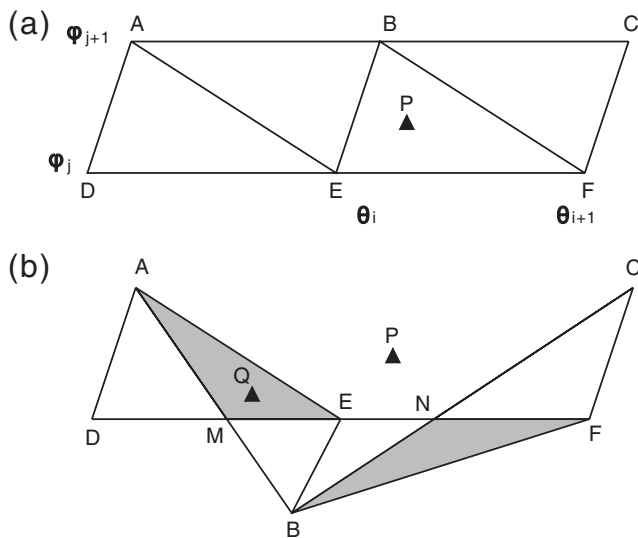


Figure 2. (a) A bunch of rays are try-shot at a proper angle range in both vertical and horizontal planes and form a set of so-called emergence triangles according a certain rule on the surface. The receiver P is located in the emergence triangle BEF . (b) The receiver Q is located in multiple triangles (the shadow zones) and the receiver P is not contained in any emergence triangles according to the same rule.

the receiver P . SIRT, falling into the catalog of bending, selects the ray whose emergence point is nearest to the receiver P (Point B in Figure 2a) and then replaces the endpoint position of the ray with that of the receiver, then the modified ray is regarded as the initial-guess ray. The subsequent iteration process terminates when the maximum modifying distance is less than a given precision (typically 1 m in this article). In general, the emergence triangles are not in the regular form (Fig. 2a) under most circumstances. For nonlinearity of the problem, the emergence triangles can overlap and appear in such form as shown in Figure 2b according to the same rule. If the receiver Q is contained in multiple triangles (the shadow zones in Fig. 2b), different initial-guess ray paths can be obtained for receiver Q and subsequent multiple ray paths may be traced by SIRT but not surely. The possibility is dependent upon the inherent characteristics of the model structure and velocity distribution, and the situation positions of the source-receiver pairs; for example, there is more possibility to handle multiple paths on a concave reflecting interface than a convex one (Fig. 3a). SIRT cannot solve multiple paths. We will not get more two-point rays than the number of the initial-guess ray paths, and thus the solution will never be complete in the presence of arrival multivaluedness, especially for the velocity models in more complicated structures and velocity distributions (Fig. 4a). If the receiver P is not contained in any emergence triangles as shown in

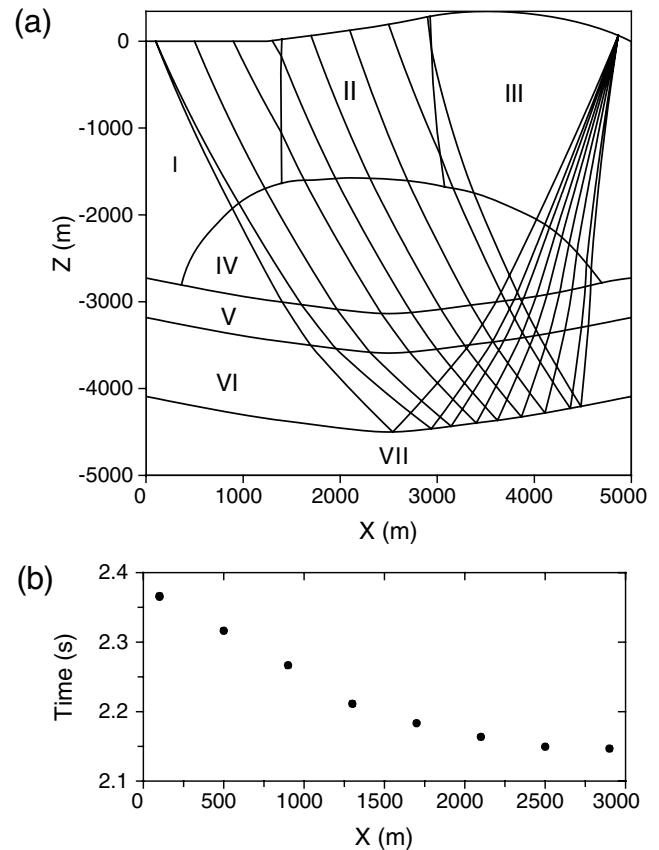


Figure 3. (a) A 2D block model (Model 1) with velocities defined in Table 1 and ray-tracing results. (b) Associated travel times.

Figure 2b, SIRT will fail due to no initial-guess paths found. If we choose much denser initial-shooting rays, the previously mentioned failure seldom occurs. However, if the receiver P is also not contained in any emergence triangles, the receiver can be regarded to be located in the shadow zone.

When the method is applied to complicated geologic settings with higher velocity discontinuities and complex shapes of structural interfaces, a new problem may arise from SIRT. Specifically, the number of intersection points in a trajectory can be increased or decreased during the course of an iteration (Xu *et al.*, 2006), therefore, the perturbed ray paths may not converge readily within maximum iteration times (typically 50–100). Similarly, if much denser initial-shooting rays are chosen, the initial-guess ray paths are closer to the true ones, and thus the method works in the most time.

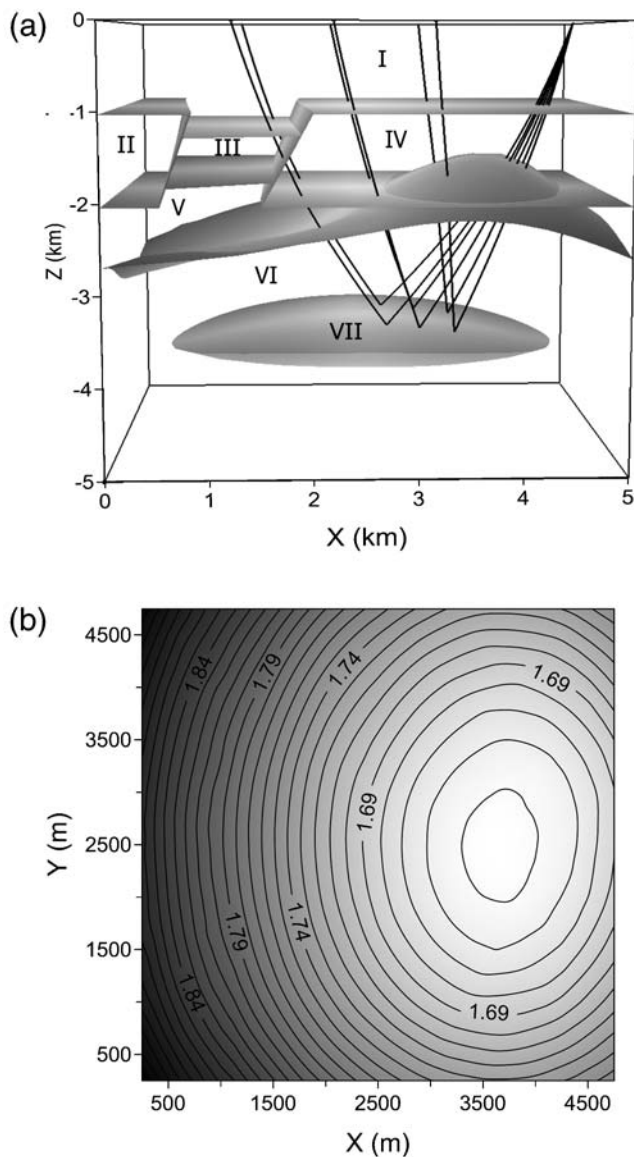


Figure 4. (a) A combination model (Model 2) with velocities defined in Table 2 and ray-tracing results. Only six ray paths are selected here for a clear display. (b) Associated travel-time isolines.

However, choosing the denser try-shooting rays costs more processing time. As a result, a proper density of try-shooting rays should be considered for computation time and efficiency of the method.

Because the try-shooting scheme for initial ray paths costs much time, in some simple velocity models such as a stratified model without violently fluctuant interfaces and without high velocity discontinuity, an initial ray path can sometimes be substituted by simple segmental circular arcs to save try-shooting time. In this circumstance, if the receiver is located in the shadow zone, the ray path will not converge usually during iteration and may or may not converge to a local minimum. A detailed comparison of SIRT with shooting and GOCAD ray-tracing scheme has been presented (Xu *et al.*, 2006). We present three block models (Figs. 3a, 4a, and 5) to illustrate SIRT in 2D and 3D heterogeneous media here. Only transmitted, reflected, and turning waves are considered in this article.

2D and 3D Ray-Tracing Examples

Figure 3a shows an intrusive mass in 2D (Model 1) with a size of 5000×5000 m. We define the upward direction as positive both in 2D and 3D. The fluctuant surface has a maximum range of 337 m. Model 1 has seven blocks (or elements) marked with the roman numerals with the associated velocity parameters defined in Table 1. Velocity parameters include original velocity v_0 and original position \mathbf{x}_0 (x_0, z_0), scale gradient constant k , and the direction of gradient \mathbf{k} , which is defined by a clockwise angle θ ranging from 0° to 360° . The lower interface is defined as the reflecting interface. Figure 3 shows the tracing results and the associated travel times plotted against the x -coordinate. Note that there are two tracing results for the first receiver, but the two travel times are close and not distinctly separated.

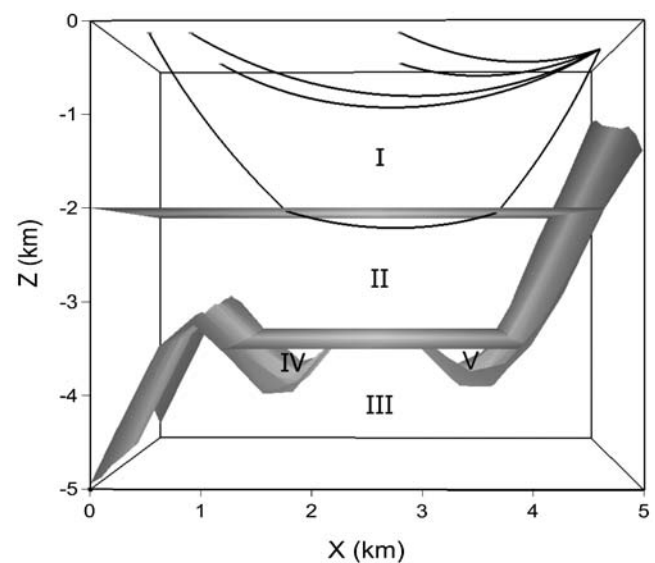


Figure 5. A stratum-crosscutting model (Model 3) with velocities defined in Table 4 and ray-tracing results of turning wave.

Table 1

2D Velocity Parameters in 7 Elements* of Model 1

Elements	V_0 , m/sec	X_0 , m	Z_0 , m	k , sec ⁻¹	θ , °
I	3000	700	0	0.6	175
II	3200	2200	0	0.5	180
III	3000	4000	0	0.6	195
IV	4200	2500	-1600	0.4	180
V	5200	2500	-3100	0.6	175
VI	6200	2500	-3600	0.7	180
VII	6800	2500	-4500	0.5	190

*Velocity parameters include an original velocity v_0 and an original position (x_0, z_0) scale gradient, constant k , and the direction of gradient vector by a clockwise angle θ , ranging from 0° to 360°.

Table 2

3D Velocity Parameters in 7 Blocks* of Model 2

Blocks	V_0 , m/sec	X_0 , m	Y_0 , m	Z_0 , m	k , sec ⁻¹	θ , °	ϕ , °
I	3000	2500	2500	0	0.7	180	0
II	3800	250	2500	-1000	0.6	170	160
III	4000	1250	2500	-1250	0.5	170	170
IV	3800	3500	2500	-1000	0.6	175	355
V	4800	1000	2500	-2000	0.5	175	75
VI	5600	2500	2500	-2000	0.7	180	0
VII	6500	2500	2500	-3700	0.8	180	0

*See Table 1 for definitions of the velocity parameters. Note that the direction of gradient vector is defined by inclination θ , ranging from 0° to 180°, and azimuth ϕ , ranging from 0° to 360°.

Figure 4a shows a combination model (Model 2), composed of normal faults, reverse faults, an intrusive mass and a lens, with a size of 5000 × 5000 × 5000 m. Model 2 has 7 blocks, 4649 triangles, and 2152 points. The velocity parameters in seven blocks marked with the roman numerals are defined in Table 2. Note that the direction of gradient \mathbf{k} is defined by inclination θ ranging from 0° to 180°, and azimuth ϕ ranging from 0° to 360°. The upper interface of the lens is defined as the reflecting interface. Figure 4 shows the tracing

Table 4

3D Velocity Parameters in 5 Blocks* of Model 3

Blocks	V_0 , m/sec	X_0 , m	Y_0 , m	Z_0 , m	k , sec ⁻¹	θ , °	ϕ , °
I	3000	2000	2500	0	0.9	180	0
II	6800	2000	2500	-2000	2.3	170	0
III	7200	2000	2500	-3500	0.5	170	170
IV	5800	1250	2500	-2000	0	0	0
V	5800	3500	2500	-2000	0	0	0

*See Table 2 for definitions of the velocity parameters.

results and the associated travel-time isolines against the x - and y -coordinates. Note that we only select six ray paths for a clear display. The velocity in this case is not in high discontinuity (Table 3) and thus the stable and continuous travel-time isolines can be obtained.

A stratum-crosscutting model (Model 3, Fig. 5) is also presented to show the action of tracing a turning ray. It has 5 blocks, 3635 triangles, and 1681 points. The velocity parameters in the five blocks are shown in Table 4 and defined in Table 2. The tracing results are shown in Figure 5. Note that only five turning rays are selected here.

To test the tracing speed, one source and 800 receivers (20 × 40 rectangle) were located on the surface. The CPU time (Pentium-M, 1.6 GHz) for SIRT in Model 2 is 8.48 sec, with a precision of 0.5 m, and for shooting is 14.62 sec with the same precision, showing that SIRT is faster in this case. Note that the precision of SIRT is defined by the largest modifying distance along the perturbed trajectory, while that of shooting is defined by the distance between the positions of the receiver and the emergence point.

Conclusions

The attractiveness of the representation of block models and a suitable segmentally iterative ray tracing have already been studied and documented. In this article, we make the model representation more realistic by extending the

Table 3

Velocity Distributions beside the Intersection Points along a Trajectory* of Model 2

Points Number	X_0 , m	Y_0 , m	Z_0 , m	Blocks Number	V_0 , m/sec	Remark
1	4750.00	2500.00	0.00	I	3000	Shot position
2	4381.23	2382.35	-999.52	I	3699.66	-
				IV	3846.16	-
3	4068.36	2284.01	-1671.59	IV	4232.01	-
				VI	5370.11	-
4	2750.56	1787.16	-3591.54	VI	6714.08	Reflecting point
5	2058.56	1411.85	-2372.96	VI	5861.07	-
				V	4951.91	-
6	1878.52	1328.06	-1999.98	V	4760.57	-
				IV	4318.58	-
7	1694.85	1242.67	-1548.15	IV	4039.33	-
				III	4089.82	-
8	1580.14	1186.98	-1238.09	III	3946.11	-
				I	3866.66	-
9	1200.00	1000.00	0.00	I	3000.00	Receiver position

*Note that the velocities are identical beside the reflecting point.

constant velocity in blocks to a generally continuous distribution, especially constant gradient distribution. This article is devoted to the development of SIRT in such heterogeneous block models, which is useful for forward modeling calculations in seismic acquisition and migration. In the constant gradient velocity model, the procedure of SIRT is similar to but more general than that in the constant velocity models. Only transmitted, reflected, and turning waves are considered in this article. Numerical tests demonstrate that SIRT is effective in implementing kinematic two-point ray tracing in complex 2D and 3D heterogeneous media.

Data and Resources

All data used in this article came from published sources listed in the references.

Acknowledgments

We gratefully acknowledge the financial support of the National Natural Science Foundation of China (40721003, 40830315, 40874041, and 40404009), National Probing Project (SinoProbe-02-02), Chinese Academy of Sciences (KZCX2-YW-132), Special Project for the Fundamental R & D of Institute of Geophysics, China Earthquake Administration (DQJB09B11), and the Knowledge Innovation Program of the Chinese Academy of Sciences. We are grateful to Fred Pollitz and an anonymous reviewer for critical comments and constructive suggestions for improvements of the manuscript. We are especially thankful to John H. Queen, Marge Queen, Shuqian Dong, and Tiejuan Zhu for helpful suggestions to improve the quality of this article.

References

- Aki, K., and P. G. Richards (1980). *Quantitative Seismology: Theory and Methods*, W. H. Freeman and Co., New York.
- Al-Chalabi, M. (1997). Time-depth relationships for multiplayer depth conversion, *Geophys. Prospect.* **45**, 715–720.
- Blias, E. A. (1985). Approximated method of determining the trajectories for the rays in 3D layered media, *Sov. Geol. Geophys.* no. 12, 82–90.
- Červený, V. (2001). *Seismic Ray Theory*, Cambridge University Press, New York.
- Červený, V., L. Klimes, and I. Psencik (1988). Complete seismic-ray tracing in three-dimensional structures, in D. J. Doornbos (Editor), *Seismological Algorithms*, Academic Press, New York, 89–168.
- Gjøystdal, H., J. E. Reinhardsen, and K. Åstebol (1985). Computer representation of complex 3-D geological structures using a new “solid modeling” technique, *Geophys. Prospect.* **33**, 195–1211.
- Guizou, J. L., J. L. Mallet, and R. Madariaga (1996). 3-D seismic reflection tomography on top of the GOCAD depth modeler, *Geophysics* **61**, no. 5, 1499–1510.
- He, Q. (2005). *Seismology Theory*, Jilin University Press (in Chinese).
- Julian, B. R., and D. Gubbins (1977). Three-dimensional seismic ray tracing, *J. Geophys.* **43**, 95–113.
- Keller, H. B., and D. J. Perozzi (1983). Fast seismic ray tracing, *SIAM J. Appl. Math.* **43**, 981–992.
- Langan, R. T., I. Lerche, and R. T. Cutler (1985). Tracing of rays through heterogeneous media: An accurate and efficient procedure, *Geophysics* **50**, 1456–1465.
- Mallet, J. L. (1989). Discrete smooth interpolation, *ACM Transactions on Graphics* **8**, 121–144.
- Mallet, J. L. (1992). Discrete smooth interpolation in geometric modeling, *Computer-Aided Design* **24**, 178–193.
- Mao, W. J., and G. W. Stuart (1997). Rapid multi-wave-type ray tracing in complex 2-D and 3-D isotropic media, *Geophysics* **62**, 298–308.
- Moser, T. J. (1991). Shortest path calculation of seismic rays, *Geophysics* **56**, 59–67.
- Pereyra, V. (1992). Two-point ray tracing in general 3-D media, *Geophys. Prospect.* **40**, 267–287.
- Pereyra, V., W. H. K. Lee, and H. B. Keller (1980). Solving two-point seismic-ray tracing problems in heterogeneous medium. Part 1. A general adaptive finite difference method, *Bull. Seismol. Soc. Am.* **70**, 79–99.
- Prothero, W., W. Taylor, and J. Eickemeyer (1988). A fast, two-point, three-dimensional raytracing algorithm using a simple step search method, *Bull. Seismol. Soc. Am.* **78**, 1190–1198.
- Ravve, I., and Z. Koren (2007). Conic velocity model, *Geophysics* **72**, U31–U46.
- Rawlinson, N., G. A. Houseman, and C. D. N. Collins (2001). Inversion of seismic refraction and wide-angle reflection traveltimes for three-dimensional layered crustal structure, *Geophys. J. Int.* **145**, 381–400.
- Sambridge, M., J. Braun, and H. McQueen (1995). Geophysical parameterization and interpolation of irregular data using natural neighbors, *Geophys. J. Int.* **122**, 837–857.
- Slotnick, M. M. (1936). On seismic computations, with applications, Part I and Part II: *Geophysics* **1**, 9–22, 299–305.
- Sun, Y. (1993). Ray tracing in 3-D media by parameterized shooting, *Geophys. J. Int.* **114**, 145–155.
- Telford, W. M., L. P. Geldart, and R. E. Sheriff (1990). *Applied Geophysics*, Second Ed., Cambridge University Press, Cambridge.
- Thurber, C., and W. Ellsworth (1980). Rapid solution of ray tracing problems in heterogeneous media, *Bull. Seismol. Soc. Am.* **70**, 1137–1148.
- Um, J., and C. Thurber (1987). A fast algorithm for two-point seismic ray tracing, *Bull. Seismol. Soc. Am.* **77**, 972–986.
- Velis, D. R., and T. J. Ulrych (1996). Simulated annealing two-point ray tracing, *Geophys. Res. Lett.* **23**, 201–204.
- Velis, D. R., and T. J. Ulrych (2001). Simulated annealing ray tracing in complex three-dimensional media, *Geophys. J. Int.* **145**, 447–459.
- Vidale, J. E. (1988). Finite-difference calculation of travel times, *Bull. Seismol. Soc. Am.* **78**, 2062–2076.
- Vidale, J. E. (1990). Finite-difference calculations of traveltimes in three dimensions, *Geophysics* **55**, 521–526.
- Vinje, V., K. Åstebol, E. Iverson, and H. Gjøystdal (1999). 3-D ray modeling by wavefront construction in open models, *Geophysics* **64**, 1912–1919.
- Vinje, V., E. Iverson, K. Åstebol, and H. Gjøystdal (1996). Estimation of multivalued arrivals in 3D models using wavefront construction—Part 1, *Geophys. Prospect.* **44**, 819–842.
- Vinje, V., E. Iverson, and H. Gjøystdal (1993). Traveltime and amplitude estimation using wavefront construction, *Geophysics* **58**, 1157–1166.
- Virieux, J., and V. Farra (1991). Ray tracing in 3-D complex isotropic media: An analysis of the problem, *Geophysics* **56**, 2057–2069.
- Xu, G., S. Wei, E. Gao, Q. Lin, X. Jiang, and K. Luo (2001). Block modeling and ray-tracing in 2-D complicated medium, *Oil Geophys. Prospect.* **36**, no. 2, 213–219 (in Chinese).
- Xu, T., G. Xu, E. Gao, Y. Li, X. Jiang, and K. Luo (2006). Block modeling and segmentally iterative ray tracing in complex 3D media, *Geophysics* **71**, T41–T51.
- Xu, T., G. Xu, E. Gao, L. Zhu, and X. Jiang (2004). Block modeling and shooting ray tracing in complex 3-D media, *Chin. J. Geophys.* **47**, no. 6, 1261–1271.
- Xu, T., Z. Zhang, A. Zhao, A. Zhang, X. Zhang, and H. Zhang (2008). Sub-triangle shooting ray tracing in complex 3D VTI media, *Journal of Seismic Exploration* **17**, 131–144.
- Zelt, C. A., and R. B. Smith (1992). Seismic traveltime inversion for 2-D crustal velocity structure, *Geophys. J. Int.* **108**, 16–34.
- Zhang, Z., and S. Klemperer (2005). West-east variation in crustal thickness in northern Lhasa block, central Tibet, from deep seismic sounding data, *J. Geophys. Res.* **110**, 1–14.

- Zhang, Z., and Y. Wang (2007). Crustal structure and contact relationship revealed from deep seismic sounding data in South China, *Phys. Earth Planet. Inter.* **165**, 114–126.
- Zhang, Z., J. Badal, Y. Li, Y. Chen, L. Yang, and J. Teng (2005). Crust-upper mantle seismic velocity structure across Southeastern China, *Tectonophysics* **395**, 137–157.
- Zhang, Z., G. Lin, J. Chen, J. M. Harris, and L. Han (2003). Inversion for elliptically anisotropic velocity using VSP reflection traveltimes, *Geophys. Prospect.* **51**, 159–166.
- Zhang, Z., G. Wang, J. Teng, and S. Klemperer (2000). CDP mapping to obtain the fine structure of the crust and upper mantle from seismic sounding data: An example for the southeastern China, *Phys. Earth Planet. Inter.* **122**, 133–146.
- Zhao, D., A. Hasegawa, and S. Horiuchi (1992). Tomographic imaging of P and S wave velocity structure beneath northeastern Japan, *J. Geophys. Res.* **97**, 19,909–19,928.
- Zhao, A., Z. Zhang, and G. Teng (2004). Minimum travel time tree algorithm for seismic ray tracing: Improvement in efficiency, *J. Geophys. Eng.* **1**, no. 4, 245–251.

Appendix A

Ray Trajectories Obtained in Terms of the Geometry Property

As Figure 1 shows, given the departure point P_0 and the end point P_1 in a constant gradient velocity distribution with gradient \mathbf{k}_1 , we can obtain the ray trajectory P_0P_1 in terms of the geometry property. For the center O_1 of the first circle lies in the plane where the velocity equals zero (Telford *et al.*, 1990; He, 2005), the center O_1 can be obtained directly by the cross of velocity-zero-plane marked with $v = 0$ and the perpendicular bisector of the line segment P_0P_1 . Thus, the distance d_0 from the departure point P_0 to the velocity-zero-plane is given by

$$d_0 = \frac{v_0}{k_1}. \quad (\text{A1})$$

Taking account of the fact that center O_1 lies in the plane as vectors \mathbf{k} and $\mathbf{P}_0\mathbf{P}_1$ yield, we can find the center \mathbf{x}_C with the following conditions

$$\begin{aligned} \|\mathbf{O}_1\mathbf{P}_0\| &= R_1, & \|\mathbf{O}_1\mathbf{P}_1\| &= R_1, & \mathbf{P}_0\mathbf{O}_1 \cdot \mathbf{P}_0\mathbf{D}_0 &= d_0^2, \\ \mathbf{k}_1 \cdot (\mathbf{O}_1\mathbf{P}_0 \times \mathbf{O}_1\mathbf{P}_1) &= 0. \end{aligned} \quad (\text{A2})$$

As a result, ray trajectory P_0P_1 can be written directly as

$$\|\mathbf{O}_1\mathbf{X}\| = R_1. \quad (\text{A3})$$

In addition, the following constraint condition should be fit, the ray P_0P_1 must lie in the plane as vectors \mathbf{k}_1 and $\mathbf{P}_0\mathbf{P}_1$ yield

$$(\mathbf{x} - \mathbf{x}_0) \cdot (\mathbf{k}_1 \times \mathbf{P}_0\mathbf{P}_1) = 0. \quad (\text{A4})$$

Appendix B

Midpoint Perturbation Formula in 3D Constant Gradient Velocity Distributions

Figure 1 shows a sketch of successive two circular arcs and the modification of the midpoint P_1 . The position in a triangle on an interface is described with two parameters as equation (5). The parameters correspond to (1, 0), (0, 1), and (0, 0) at the three vertices. We define two constant gradient velocity blocks with the gradient vector in the upper block \mathbf{k}_1 and in the lower \mathbf{k}_2 . The wave velocity at the departure point P_0 is v_0 and at the end point P_2 is v_3 , velocities are v_1 and v_2 at the midpoint P_1 beside the interface. Then the travel time through the two arcs can be described as

$$\begin{aligned} T &= t(P_0, P_1) + t(P_1, P_2) \\ &= \frac{1}{k_1} \text{arc cosh } p_1 + \frac{1}{k_2} \text{arc cosh } p_2, \end{aligned} \quad (\text{B1a})$$

with

$$\begin{aligned} p_1 &= 1 + \frac{k_1^2 r_1^2}{2v_0(\mathbf{x}^{(1)})v_1(\mathbf{x}^{(2)})}, \\ p_2 &= 1 + \frac{k_2^2 r_2^2}{2v_2(\mathbf{x}^{(2)})v_3(\mathbf{x}^{(3)})}, \end{aligned} \quad (\text{B1b})$$

where

$$\begin{aligned} k_1 &= \|\mathbf{k}_1\|, & k_2 &= \|\mathbf{k}_2\|, & r_1 &= \|\mathbf{x}^{(2)} - \mathbf{x}^{(1)}\|, \\ r_2 &= \|\mathbf{x}^{(2)} - \mathbf{x}^{(3)}\|. \end{aligned} \quad (\text{B2})$$

The conditions for stationary travel time are

$$\left. \frac{\partial T}{\partial s} \right|_{(s=s^*, t=t^*)} = 0, \quad \left. \frac{\partial T}{\partial t} \right|_{(s=s^*, t=t^*)} = 0, \quad (\text{B3})$$

where s^* and t^* are the improved midpoint coordinates. Another form is

$$\begin{aligned} \left(k_2 \sqrt{p_2^2 - 1} \frac{\partial p_1}{\partial s} + k_1 \sqrt{p_1^2 - 1} \frac{\partial p_2}{\partial s} \right) \Big|_{(s=s^*, t=t^*)} &= 0, \\ \left(k_2 \sqrt{p_2^2 - 1} \frac{\partial p_1}{\partial t} + k_1 \sqrt{p_1^2 - 1} \frac{\partial p_2}{\partial t} \right) \Big|_{(s=s^*, t=t^*)} &= 0. \end{aligned} \quad (\text{B4})$$

Making Taylor series expansions of variables in equation (B4) and retaining only the first-order perturbation,

$$\begin{aligned}
& \sqrt{p_1^2 - 1} \Big|_{(s=s^*, t=t^*)} \\
&= \sqrt{p_1^2 - 1} + \frac{p_1}{\sqrt{p_1^2 - 1}} \frac{\partial p_1}{\partial x_i} (x_{is} \Delta s + x_{it} \Delta t), \\
& \frac{\partial p_1}{\partial s} \Big|_{(s=s^*, t=t^*)} \\
&= \frac{\partial p_1}{\partial x_i} x_{is} + \left(\frac{\partial^2 p_1}{\partial x_i \partial x_j} x_{is} x_{js} + \frac{\partial p_1}{\partial x_i} x_{iss} \right) \Delta s \\
&+ \left(\frac{\partial^2 p_1}{\partial x_i \partial x_j} x_{is} x_{jt} + \frac{\partial p_1}{\partial x_i} x_{ist} \right) \Delta t. \tag{B5}
\end{aligned}$$

Note that not all expansions of variables are presented here.

Elements in equation (B4) are substituted into equation (B5). Expanding equation (B4) and retaining only the first-order perturbation results in the ultimate perturbation formula

$$\Delta s = \frac{U_{13} U_{22} - U_{23} U_{12}}{U_{11} U_{22} - U_{12} U_{21}}, \quad \Delta t = \frac{U_{11} U_{23} - U_{21} U_{13}}{U_{11} U_{22} - U_{12} U_{21}}, \tag{B6}$$

where

$$\begin{aligned}
U_{11} &= k_2 (e_2 A_s^{(1)} A_s^{(3)} + f_2 B_{ss}^{(1)}) + k_1 (e_1 A_s^{(1)} A_s^{(3)} + f_1 B_{ss}^{(3)}), \\
U_{12} &= k_2 (e_2 A_s^{(1)} A_t^{(3)} + f_2 B_{st}^{(1)}) + k_1 (e_1 A_t^{(1)} A_s^{(3)} + f_1 B_{st}^{(3)}), \\
U_{13} &= -(k_2 f_2 A_s^{(1)} + k_1 f_1 A_s^{(3)}), \\
U_{21} &= k_2 (e_2 A_t^{(1)} A_s^{(3)} + f_2 C_{ts}^{(1)}) + k_1 (e_1 A_s^{(1)} A_t^{(3)} + f_1 C_{ts}^{(3)}), \\
U_{22} &= k_2 (e_2 A_t^{(1)} A_t^{(3)} + f_2 C_{tt}^{(1)}) + k_1 (e_1 A_t^{(1)} A_t^{(3)} + f_1 C_{tt}^{(3)}), \\
U_{23} &= -(k_2 f_2 A_t^{(1)} + k_1 f_1 A_t^{(3)}), \quad e_1 = \frac{p_1}{\sqrt{p_1^2 - 1}}, \\
e_2 &= \frac{p_2}{\sqrt{p_2^2 - 1}}, \quad f_1 = \sqrt{p_1^2 - 1}, \quad f_2 = \sqrt{p_2^2 - 1}, \\
A_s^{(1)} &= Q_i^{(1)} x_{is}^{(2)}, \quad A_t^{(1)} = Q_i^{(1)} x_{it}^{(2)}, \quad A_s^{(3)} = Q_i^{(3)} x_{is}^{(2)}, \\
A_t^{(3)} &= Q_i^{(3)} x_{it}^{(2)}, \quad B_{ss}^{(1)} = Q_i^{(1)} x_{iss}^{(2)} + R_{ij}^{(1)} x_{is}^{(2)} x_{js}^{(2)}, \\
B_{st}^{(1)} &= Q_i^{(1)} x_{ist}^{(2)} + R_{ij}^{(1)} x_{is}^{(2)} x_{jt}^{(2)}, \\
B_{ss}^{(3)} &= Q_i^{(3)} x_{iss}^{(2)} + R_{ij}^{(3)} x_{is}^{(2)} x_{js}^{(2)}, \\
B_{st}^{(3)} &= Q_i^{(3)} x_{ist}^{(2)} + R_{ij}^{(3)} x_{is}^{(2)} x_{jt}^{(2)}, \\
C_{ts}^{(1)} &= Q_i^{(1)} x_{its}^{(2)} + R_{ij}^{(1)} x_{it}^{(2)} x_{js}^{(2)}, \\
C_{tt}^{(1)} &= Q_i^{(1)} x_{itt}^{(2)} + R_{ij}^{(1)} x_{it}^{(2)} x_{jt}^{(2)}, \\
C_{ts}^{(3)} &= Q_i^{(3)} x_{its}^{(2)} + R_{ij}^{(3)} x_{it}^{(2)} x_{js}^{(2)}, \\
C_{tt}^{(3)} &= Q_i^{(3)} x_{itt}^{(2)} + R_{ij}^{(3)} x_{it}^{(2)} x_{jt}^{(2)},
\end{aligned} \tag{B7a}$$

$$\begin{aligned}
Q_i^{(1)} &= \frac{k_1^2}{2v_0} \frac{2(x_i^{(2)} - x_i^{(1)})v_1 - r_1^2 k_i^{(1)}}{v_1^2}, \\
Q_i^{(3)} &= \frac{k_2^2}{2v_3} \frac{2(x_i^{(2)} - x_i^{(3)})v_2 - r_2^2 k_i^{(2)}}{v_2^2}, \\
R_{ij}^{(1)} &= \frac{k_1^2}{v_0} \left(\frac{\delta_{ij} v_1 - (x_i^{(2)} - x_i^{(1)})k_j^{(1)} - (x_j^{(2)} - x_j^{(1)})k_i^{(1)}}{v_1^2} \right. \\
&\quad \left. + \frac{r_1^2 k_i^{(1)} k_j^{(1)}}{v_1^3} \right), \\
R_{ij}^{(3)} &= \frac{k_2^2}{v_3} \left(\frac{\delta_{ij} v_2 - (x_i^{(2)} - x_i^{(3)})k_j^{(2)} - (x_j^{(2)} - x_j^{(3)})k_i^{(2)}}{v_2^2} \right. \\
&\quad \left. + \frac{r_2^2 k_i^{(2)} k_j^{(2)}}{v_2^3} \right), \\
k_i^{(1)} &= \mathbf{k}_1 \cdot \mathbf{e}_i, \quad k_i^{(2)} = \mathbf{k}_2 \cdot \mathbf{e}_i, \quad v_0 = v_0(\mathbf{x}^{(1)}), \\
v_1 &= v_1(\mathbf{x}^{(2)}), \quad v_2 = v_2(\mathbf{x}^{(2)}), \quad v_3 = v_3(\mathbf{x}^{(3)}), \\
\delta_{ij} &= \begin{cases} 1, & i = j \\ 0, & i \neq j \end{cases}, \quad x_{is}^{(2)} = \frac{\partial x_i^{(2)}}{\partial s}, \quad x_{it}^{(2)} = \frac{\partial x_i^{(2)}}{\partial t}, \\
x_{iss}^{(2)} &= \frac{\partial^2 x_i^{(2)}}{\partial s^2}, \quad x_{ist}^{(2)} = x_{its}^{(2)} = \frac{\partial^2 x_i^{(2)}}{\partial s \partial t}, \\
x_{itt}^{(2)} &= \frac{\partial^2 x_i^{(2)}}{\partial t^2} \tag{B7b}
\end{aligned}$$

State Key Laboratory of Lithosphere Evolution
Institute of Geology and Geophysics
Chinese Academy of Sciences
Beijing, China, 100029
(T.X., Z.Z.)

Institute of Disaster Prevention Science and Technology
Hebei, China, 101601
(E.G.)

School of Earth and Space Sciences
University of Science and Technology of China
Anhui, China, 230026
(G.X.)

Institute of Geophysics
China Earthquake Administration
Beijing, China, 100081
(L.S.)